

Pre-retinal delivery of recombinant adeno-associated virus vector significantly improves retinal transduction efficiency

Hanmeng Zhang,^{1,2} Benjamin S. Sajdak,^{1,2,3} Dana K. Merriman,⁴ Joseph Carroll,^{1,2} and Daniel M. Lipinski^{1,2,5}

¹Cell Biology, Neurobiology and Anatomy, Medical College of Wisconsin, Milwaukee, WI 53226, USA; ²Department of Ophthalmology and Visual Sciences, Medical College of Wisconsin, 925 N 87th Street, Milwaukee, WI 53226, USA; ³Morgridge Institute for Research, Madison, WI 53715, USA; ⁴Department of Biology, University of Wisconsin Oshkosh, Oshkosh, WI 54901, USA; ⁵Nuffield Laboratory of Ophthalmology, University of Oxford, Oxford OX1 2JD, UK

Intravitreal injection is the most widely used injection technique for ocular gene delivery. However, vector diffusion is attenuated by physical barriers and neutralizing antibodies in the vitreous. The 13-lined ground squirrel (13-LGS), as in humans, has a larger relative vitreous body volume than the more common rodent models such as rats and mice, which would further reduce transduction efficiency with the intravitreal injection route. We report here a “pre-retinal” injection approach that leads to detachment of the posterior hyaloid membrane and delivers vector into the space between vitreous and inner retina. Vectors carrying a ubiquitously expressing mCherry reporter were injected into the deep vitreous or pre-retinal space in adult wild-type 13-LGSs. Then, adeno-associated virus (AAV)-mediated mCherry expression was evaluated with non-invasive imaging, immunofluorescence, and flow cytometry. Compared to deep vitreous delivery, pre-retinal administration achieved pan-retinal gene expression with a lower vector dose volume and significantly increased the number of transduced cone photoreceptors. These results suggest that pre-retinal injection is a promising tool in the development of gene therapy strategies in animal models and is a potential approach for use in human research, particularly in younger individuals with an intact posterior hyaloid membrane and stable vitreous.

INTRODUCTION

In pre-clinical animal studies and human clinical trials, the transfer of genetic material to cells of the retina is routinely achieved through the intraocular injection of viral vectors, such as recombinant adeno-associated virus (rAAV). Depending on the cell types being targeted, vector is typically injected into either the subretinal space—a potential volume located between the photoreceptors and the retinal pigment epithelium (RPE)—or the vitreous humor—a semi-solid, colorless gel that is encapsulated within a membrane and fills the posterior chamber of the globe.

Subretinal injection of rAAV leads to localized and highly efficient transduction of photoreceptors and RPE within the area of retinal detachment; however, the surgery is technically challenging,

requiring precise localization of the cannula tip into a potential space and the hydro-dissection of apposing tissue planes, which can cause permanent damage and lead to the development of severe vision-threatening complications.¹ By contrast, intravitreal injection is a relatively straightforward surgical technique, involving delivery of fluid into the deep vitreous without the cannula tip contacting either the retinal surface or posterior lens capsule, and, as such, is employed routinely in the clinical treatment of neovascular ocular disease where repetitive (up to monthly) administration of pharmacological agents is indicated.^{2–4} Intravitreal injection can also be used for the delivery of rAAV, but transduction efficiency is typically poor owing to the failure of vector particles to reach the neural retina. Instead, they become diluted in the vitreous humor or bind irreversibly to the internal limiting membranes (ILMs).^{5–7}

Although numerous attempts to increase transduction efficiency from the vitreous aspect have been made in the past two decades by modifying rAAV vectors through mutagenesis or rational design, particularly for the targeting photoreceptor cells, transduction remains more efficient after subretinal delivery, despite its increased surgical risk.^{8–14} More recently, transduction efficiency after intravitreal injection of rAAV was shown to improve substantially with the use of a technique termed “para-retinal administration,” wherein the injection cannula/needle tip is advanced into the deep vitreous closer to the ILM prior to injection. Para-retinal administration has the benefits of limiting vector diffusion into the vitreous humor and minimizing the potential for immunogenicity toward free vector particles.¹⁵

Building upon this concept, here we demonstrate that rAAV transduction efficiency might be improved further by performing “pre-retinal administration,” a technique wherein the cannula is advanced beyond the vitreous body into another potential space located

Received 8 January 2021; accepted 7 June 2021;
<https://doi.org/10.1016/j.omtm.2021.06.005>.

Correspondence: Daniel M. Lipinski, Department of Ophthalmology and Visual Sciences, Medical College of Wisconsin, 925 N 87th Street, Milwaukee, WI 53226, USA.

E-mail: dlipinski@mcw.edu



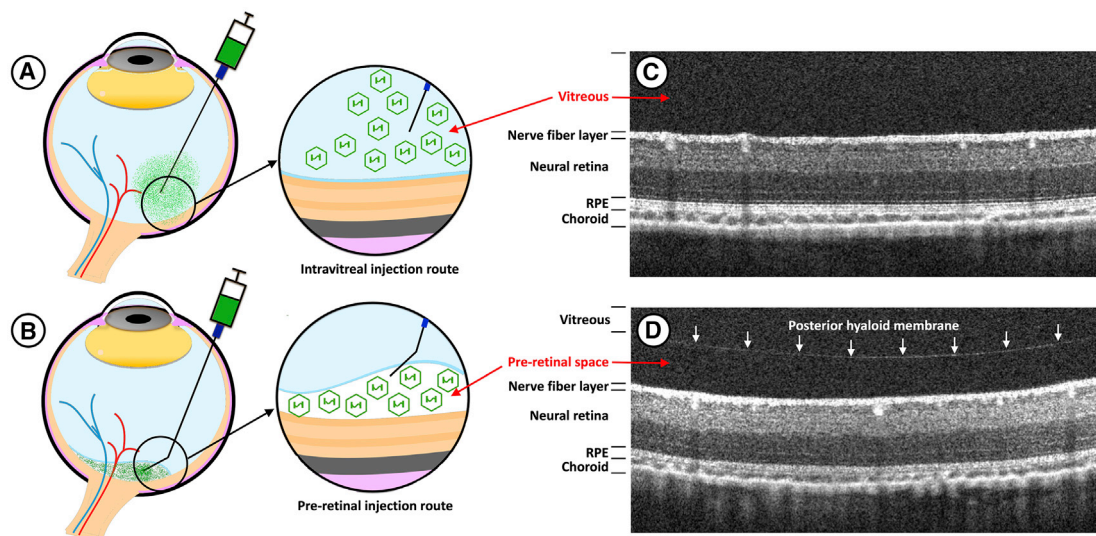


Figure 1. Traditional intravitreal injection versus pre-retinal injection approach

(A) Traditional intravitreal injection route by placing needle tip in the vitreous body. Zoom-in image: vectors are released above the posterior hyaloid membrane and diffused in the vitreous body. (B) Pre-retinal injection route by placing needle tip underneath the posterior hyaloid membrane. Zoom-in image: vectors are restricted to the pre-retinal space that is adjacent to the inner retina. (C and D) Volume OCT scanning of the visual streak area immediately after intravitreal injection (C) or pre-retinal injection (D). Detached hyaloid membrane (white arrow) is observed in the pre-retinal administration (D).

between the posterior hyaloid membrane of the vitreous and the ILM of the neural retina. Here we have applied pre-retinal administration to the thirteen-lined ground squirrel (13-LGS), a small cone-dominant, diurnal rodent with large eyes whose retinal structure and function have been established previously by non-invasive imaging and electroretinography (ERG).^{16–18} We show that injection of rAAV into the pre-retinal space substantially alters vector tropism and significantly increases transduction of cone photoreceptors, while requiring an overall lower vector dose than the traditional deep vitreous injection approach. In addition to providing a promising alternative vector delivery route in animal models and potentially human patients, these findings directly expand the experimental utility of the 13-LGS as a valuable model for retinal disease research.

RESULTS

Pre-retinal injection of HBSS leads to permanent detachment of the posterior hyaloid membrane

The para-retinal injection technique described recently by Zeng et al. demonstrated that limiting vector diffusion throughout the vitreous by releasing rAAV immediately proximal to the ILM leads to significantly improved retinal transduction compared to a “traditional” intravitreal delivery approach (Figure 1A).¹⁵ Building on the hypothesis that vector diffusion is a critical factor limiting transduction efficiency, we used a 13-LGS model to develop a *pre*-retinal injection technique, wherein the tip of the injection cannula is advanced *beyond* the vitreous body into an enclosed space located between the posterior hyaloid membrane and the ILM (Figure 1B; Figure S1; Video S1). Optical coherence tomography (OCT) imaging performed immediately after pre-retinal injection of 20 μ L of Hank’s balanced salt solution (HBSS) revealed complete detachment and visualization

of the posterior hyaloid membrane in all three animals ($n = 6$ eyes, Table 1; Figure 1D, white arrows). Repetitive OCT demonstrated that the posterior hyaloid membrane did not reattach for a period of at least 9 weeks, indicating that detachment may be permanent once induced (Figure S2, red arrow). No changes to any other retinal layers were observed, indicating that delivery of fluid into the pre-retinal space and long-term detachment of the posterior hyaloid membrane are well tolerated in the 13-LGS. In one pre-retinal injected eye, hyper-reflective puncta were observed in the vitreous via OCT, indicative of mild inflammation typified by infiltration of immune cells (e.g., macrophages) (Figure S2, orange arrows).

Pre-retinal injection of rAAV leads to significantly improved retinal transduction compared to deep vitreous intravitreal delivery in the 13-LGS

Having established that the posterior hyaloid membrane can be safely and reproducibly detached in the 13-LGS model, we sought to assess whether delivery of rAAV into the pre-retinal space leads to improved transduction efficiency or altered retinal tropism compared to injection via a traditional intravitreal delivery approach. A red fluorescent reporter gene (mCherry) driven by a ubiquitously expressing chicken beta actin (CBA) promoter was packaged at high titer (1×10^{13} vector genomes [vg] per mL) into rAAV2/2[*MAX*], a capsid mutant serotype containing multiple point mutations and the 7m8 peptide insertion that has been shown to effectively transduce the neural retina after intravitreal delivery in mice.^{10,13,14} Adult wild-type 13-LGSs were divided randomly between three cohorts, with cohorts 1 and 2 receiving intravitreal injections of rAAV2/2[*MAX*].CBA.mCherry at either low (20 μ L, 2×10^{11} vg) or high (60 μ L, 6×10^{11} vg) dose volume; 13-LGSs in cohort 3 received pre-retinal injections at the lowest dose

Table 1. Animal grouping and usage details

Experiments	Number of eyes	Treatment	Usage	
cohorts 1—20 μ L AAV2/2[<i>MAX</i>].CBA.mCherry intravitreal injection group (N = 2; F = 1, M = 1)	n = 3	AAV	SLO, FC	
	n = 1	AAV	SLO, IF	
cohorts 2—60 μ L AAV2/2[<i>MAX</i>].CBA.mCherry intravitreal injection group (N = 4; F = 2, M = 2)	n = 3	AAV	SLO, FC	
	n = 1	AAV	SLO, IF	
Evaluation of transduction efficiency (N = 17; Female = 9 Male = 8)	n = 4	<i>For unrelated experiment</i>		
	cohorts 3—20 μ L AAV2/2[<i>MAX</i>].CBA.mCherry pre-retinal injection group (N = 4; F = 2, M = 2)	n = 4	AAV	SLO, FC
		n = 3	AAV	SLO, IF
		n = 1	N/A	FC (for gating)
	Non-injection (N = 1, M)	n = 2	N/A	FC (for gating)
cohorts 4—AAV2/5.CBA.mCherry intravitreal and pre-retinal injection groups (N = 6; F = 4, M = 2)	n = 11	AAV	ERG, SLO, OCT, IF	
Sham pre-retinal injection (N = 3, Female)	n = 6	HBSS	OCT	

FC, flow cytometry; IF, immunofluorescence; F, female; M, male.

(2×10^{11} vg) and volume (20 μ L) only, as this is the maximum volume tolerated in this space (Table 1). Intravitreal and pre-retinal injected animals underwent post-operative OCT imaging immediately following removal of the injection cannula to confirm vector delivery to the appropriate anatomical location and exclude the possibility of vector infiltration into the sub-retinal space. Four to eight weeks post-injection, all animals were imaged *in vivo* with a confocal scanning laser ophthalmoscope (cSLO) in order to assess gross retinal morphology and the distribution of mCherry expression throughout the neural retina. Near-infrared (NIR) imaging of the fundus (Figures 2A–2C) revealed no changes in reflectivity in either intravitreal or pre-retinal injected animals, indicating an absence of injection-related damage.

In vivo fluorescence imaging using a custom equipped 561 nm sapphire laser and a standardized gain setting (sensitivity = 90) revealed mCherry expression in the retina of all rAAV2/2[*MAX*].CBA.mCherry-injected animals (Figures 2D–2F). As expected, mCherry fluorescence (red signal) increased in strength and distribution as a function of dose in intravitreal injected eyes, ranging from sporadic transduction of central retinal cells in eyes receiving 20 μ L (2×10^{11} vg) of rAAV (Figure 2D) to widespread expression following injection of 60 μ L (6×10^{11} vg) of rAAV (Figure 2E). By contrast, eyes injected pre-retinally with 20 μ L (2×10^{11} vg) of rAAV demonstrated pan-retinal mCherry expression (Figure 2F) that was substantially greater in intensity (i.e., saturating) than the signal observed in eyes receiving 60 μ L of rAAV via an intravitreal route (Figure 2E). Thus, pre-retinal administration effectively increased transduction efficiency while simultaneously lowering vector dose.

To determine the extent of retinal transduction and to evaluate whether pre-retinal delivery of rAAV alters vector tropism, globes from animals with different injection routes and vector doses (20 μ L and 60 μ L intravitreal or 20 μ L pre-retinal) were harvested and sectioned medially through the horizontal optic nerve head and

cone-rich visual streak.¹⁹ mCherry expression with a 20 μ L intravitreal injection volume was largely limited to ganglion cells and inner retinal neurons, with relatively few transduced photoreceptors (Figures 3A 3B, 3G, and 3H). In high-dose (60 μ L, 6×10^{11} vg) intravitreally injected animals, mCherry expression was observed to be substantially greater in the ganglion cell layer (GCL), but there remained relatively few transduced cells in either the inner nuclear layer (INL) or photoreceptor layer (ONL) (Figures 3C, 3D, 3I, and 3J). By contrast, rAAV delivered into the pre-retinal space exhibited substantially altered tropism, with greatly increased numbers of mCherry-expressing inner retinal neurons and photoreceptors and ganglion cells, indicating that pre-retinal administration greatly increased rAAV penetrance into the retina (Figures 3E, 3F, 3K, and 3L and Figures 4B–4E), albeit not to the level of the RPE, which was not observed to be transduced in any eyes. In the majority of pre-retinal injected eyes, transduction was observed to be pan-retinal, with strong transduction in retinal layers extending from the optic nerve head to the periphery (Figure 4A). Interestingly, although overall transduction efficiency was higher in pre-retinal injected eyes, there is variability between injections, with some retinal areas exhibiting strong transduction of the GCL and INL with minimal involvement of the ONL (Figures 3E, 3F, 3K, and 3L), while other areas show strong fluorescence in photoreceptors, but with minimal evidence of inner retinal transduction (Figures 4B–4E).

To confirm that pre-retinal injection of rAAV resulted in increased transduction of cone photoreceptors—which comprise ~85% of outer retinal neurons in the 13-LGS model—we quantified the number of MWS and SWS opsin-positive cells that co-expressed mCherry by performing flow cytometry on papain-dissociated retinæ. Uninjected 13-LGS eyes without immunostaining (Figures 5A and 5B) or stained individually for the presence of MWS (Figure 5C) or SWS (Figure 5D) opsin served as gating controls. Intravitreal injection of 60 μ L of rAAV2/2[*MAX*].CBA.mCherry (6×10^{11} vg) resulted in only modest transduction of photoreceptors, with $4.37\% \pm 2.27\%$ and

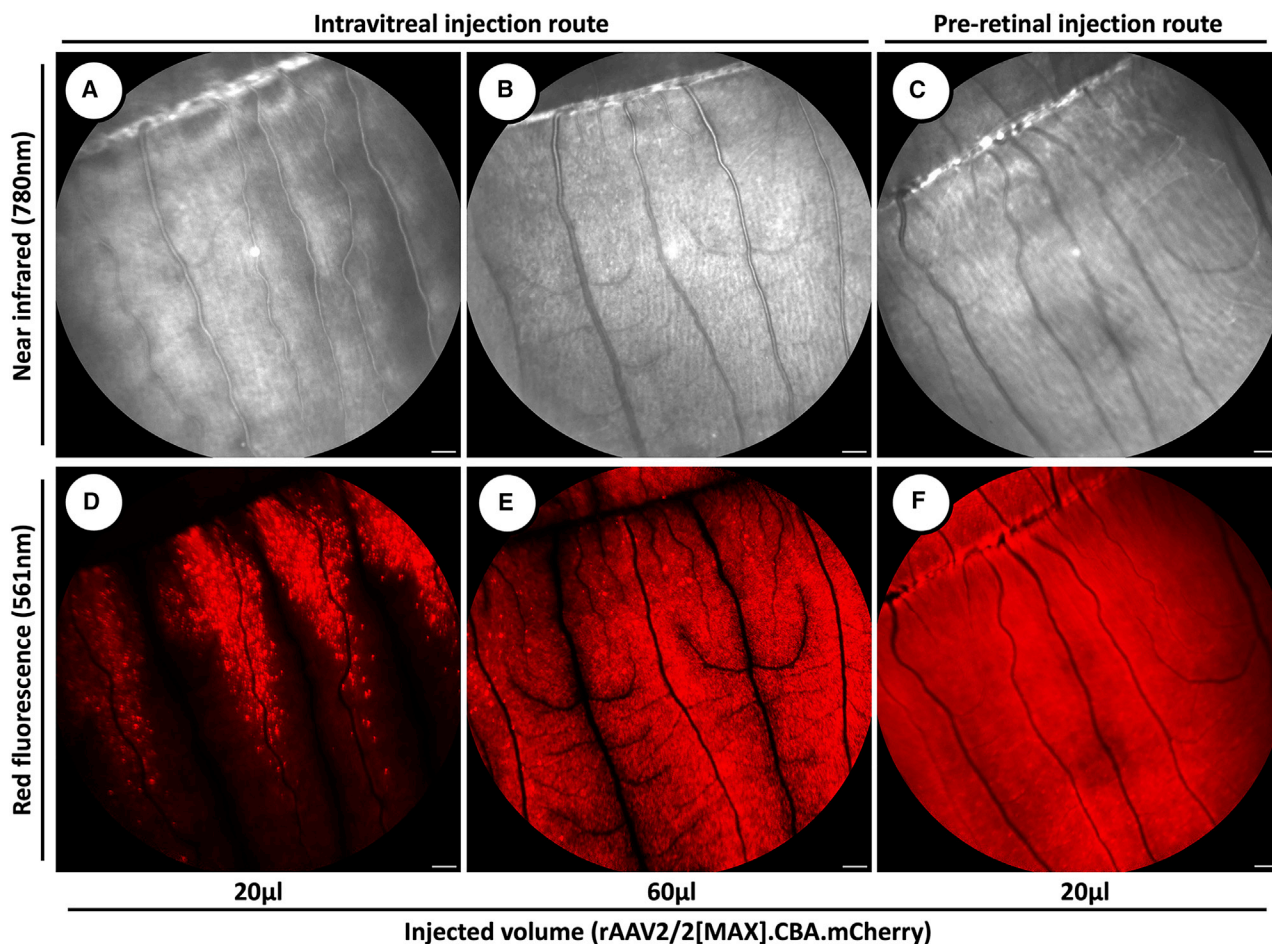


Figure 2. csLO fundus images in 13-LGSs with intravitreal or pre-retinal rAAV2/2[*MAX*].CBA.mCherry administration

(A–C) Near-infrared (780 nm) fundus image in 13-LGS with 20 μ L vector intravitreal injection (A), 60 μ L vector intravitreal injection (B), and 20 μ L vector pre-retinal injection (C). (D–F) Red fluorescence (561 nm) fundus image in 13-LGS with 20 μ L vector intravitreal injection (D), 60 μ L vector intravitreal injection (E), and 20 μ L vector pre-retinal injection (F). mCherry signal is mainly distributed in the visual streak area with 20 μ L vector delivery (D) and extends to the whole retina along with vessels with 60 μ L vector administration (E). Pre-retinal injection (F) shows a strong and pan-retinal mCherry signal with lower vector dose volume requirement. Scale bars, 1 mm.

4.66% \pm 1.01% of dissociated cells co-expressing mCherry and either MWS (Figure 5E) or SWS (Figure 5F) opsin, respectively. By contrast, pre-retinal injection of 20 μ L of rAAV2/2[*MAX*].CBA.mCherry (2×10^{11} vg) resulted in significantly greater transduction of both MWS (14.2% \pm 3.21%, $p = 0.0011$)- and SWS (16.63% \pm 3.67%, $p = 0.0164$)-expressing photoreceptors (one-way ANOVA with Tukey post hoc assay). Together, these data strongly indicate that delivery of rAAV into the pre-retinal space leads to significantly improved tissue penetration and photoreceptor transduction, while simultaneously limiting the vector dose required.

Electroretinography reveals no evidence of procedure-related damage following pre-retinal injection of rAAV

To ensure that visual function is preserved after pre-retinal and intravitreal injection procedures, we performed full-field ERG (ffERG) on 13-LGSs before, 1 week and 4 weeks after 20 μ L intravitreal injection ($n = 3$ eyes), 60 μ L intravitreal injection ($n = 5$ eyes), or 20 μ L vector

pre-retinal injection ($n = 3$ eyes) of rAAV. The amplitudes of the dark-adapted a- and b-waves, which reflect the function of photoreceptors and ON-bipolar cells respectively, and light-adapted b-wave were observed to be slightly but not significantly reduced 1-week post-injection in intravitreal injected eyes but not in pre-retinal injected eyes (Figures 6A–6F). Four weeks post-injection all waveforms (dark and light adapted) were observed to be comparable to pre-injection amplitudes in both the intravitreal and pre-retinal injection groups, with no significant differences at any light intensity (-4 to $1 \log \text{cd} \cdot \text{s}/\text{m}^2$) evaluated ($p > 0.05$, all comparisons, two-way ANOVA with Tukey post hoc assay). Together, these data strongly indicate that the pre-retinal injection route is tolerated equally as well as the more commonly utilized intravitreal delivery approach.

DISCUSSION

This study presents a pre-retinal injection technique and demonstrates that delivery of viral vector into the potential space between

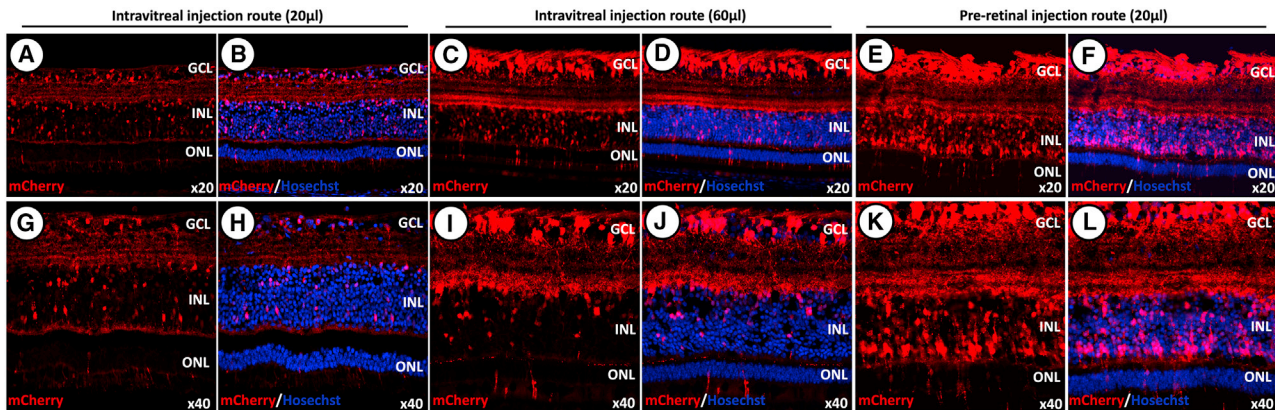


Figure 3. Evaluation of transduction efficiency in 13-LGSs with intravitreal or pre-retinal vector delivery by immunostaining

Immunofluorescence images of mCherry signal (A, C, E, G, I, K) with counterstaining of Hoechst (B, D, F, H, J, L) at 20 \times objective (A–F) and 40 \times objective (G–L) magnifications. mCherry signal is highly enhanced in the ganglion cell layer (GCL) and inner nuclear layer (INL) with pre-retinal administration.

the ILM and posterior hyaloid membrane significantly increases transduction efficiency and alters tropism compared to when vector is injected into the deep vitreous. Specifically, we propose that delivery of rAAV into the pre-retinal space effectively circumvents two major barriers preventing effective transduction from the vitreous aspect.

First, delivery of rAAV into a constrained potential space bounded by two membranes is likely to substantially limit vector diffusion throughout the vitreous and increase the effective dose received by cells of the retina. Although this had the effect of reducing the absolute volume of vector that could be delivered, we nevertheless observed significantly greater M- and S-cone photoreceptor transduction following pre-retinal injection of 20 μ L (containing 2×10^{11} vg) of rAAV, compared to when three times that dose (60 μ L, containing 6×10^{11} vg) was administered into the deep vitreous (Figures 3, 4, and 5; Table 2). Importantly, although evading host immunity is not a major concern when working with naive animals in a laboratory setting, delivery of rAAV into the pre-retinal space may also help minimize exposure of the virion to neutralizing antibodies and immune cells located within the vitreous/aqueous and may limit vector biodistribution outside of the globe. Although this was not evaluated as part of the current study, both vector neutralization and ectopic distribution are substantial concerns, especially when administering vector in subjects with pre-existing immunity ($\sim 50\%$ of the human population, depending on serotype), and so the potential that delivering vector into the pre-retinal space helps ameliorate these interactions may be an important topic for future study.^{6,20,21} Indeed, whereas detachment of the posterior hyaloid membrane persisted for a period of several weeks and may be permanent, injection of rAAV into the pre-retinal space appears to be well tolerated, with only one eye exhibiting hyper-reflective foci—likely infiltrating macrophages—within the vitreous on OCT imaging (Figure S2).²²

Second, the uptake of rAAV vectors into the retina from the vitreous is critically dependent upon the interaction of the virus capsid

with its ligand, which in the case of rAAV2/2 is heparin sulfate proteoglycan (HSPG), a major constituent of the ILM.²³ This interaction is complex, however, where it has been demonstrated that partially reducing the affinity of the rAAV2/2 capsid through targeted mutagenesis of specific surface residues leads to increased retinal transduction efficiency, but ablating HSPG binding entirely prevents transduction following intravitreal delivery.²⁴ Relatedly, it has also been demonstrated that altering the composition of the ILM to partially deplete HSPG through enzymatic digestion (e.g., heparinase, pronase E) also leads to increased transduction efficiency and altered tropism following intravitreal injection of rAAV.^{25–27} As such, it is clear that for rAAV2-based vectors to successfully penetrate the retina, they must adhere to HSPG in the ILM and subsequently traverse the membrane without becoming irreparably bound. We propose that the pre-retinal injection route described here is ideally designed to facilitate this interaction by effectively trapping the majority of vector particles against the ILM surface, leading to increased numbers of virions binding HSPG and being transported into the neural retina. This is in direct contrast to intravitreal delivery of rAAV, where the majority of virions likely remain suspended in the vitreous humor and do not reach the ILM surface. Another possibility is that detaching the posterior hyaloid membrane also serves to deplete HSPG from the ILM, thus lowering the overall affinity and preventing irreversible adhesion of vector particles. Although it remains an open question whether the posterior hyaloid membrane is indeed part of the ILM or a separate anatomical structure, Fincham et al. found that collagen IV and laminin, two other major components of ILM, are distributed densely on the posterior hyaloid membrane after detachment.²⁸ Although their study did not look directly at other basement membrane components, it would be logical to expect that, if collagen IV and laminin are sheared from the ILM during detachment, that HSPG is also potentially removed.²⁹

As pre-retinal injection is proposed to increase transduction efficiency partly through limiting vector diffusion throughout the

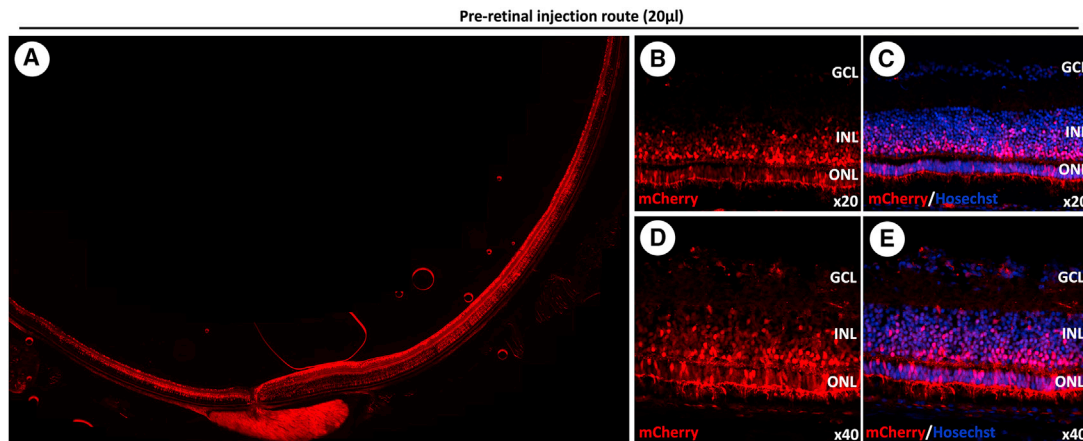


Figure 4. Pan-retinal mCherry expression following pre-retinal vector administration

(A) Native mCherry fluorescence signal is observed pan-retinally after pre-retinal rAAV vector administration. (B–E) Immunostaining for mCherry signal (B and D) with nuclear counterstaining using Hoechst (C and E) at 20 \times objective (B and C) and 40 \times objective (D and E) magnifications. Some areas of pre-retinal injection exhibited strong transduction of cells in the inner and outer retina with only minimal ganglion cell transduction.

vitreous humor and by circumventing the posterior hyaloid membrane, we did briefly evaluate whether this delivery route might also improve transduction of rAAV serotypes that do not use HSPG as a primary receptor, such as rAAV2/5, which binds strongly to platelet-derived growth factor receptor (PDGFR), a receptor found extensively on photoreceptors and RPE but not in the ILM.^{5,30–32} Unsurprisingly, injection of rAAV2/5.CBA.mCherry either intravitreally (20 μ L or 60 μ L) or pre-retinally (20 μ L) failed to result in retinal transduction, as evidenced by an absence of mCherry expression on both *in vivo* cSLO imaging and postmortem histology (Figure S3). This is in agreement with previous studies that have demonstrated that complete removal of the ILM (and presumably posterior hyaloid membrane) via peeling is necessary to facilitate transduction of the retina using rAAV2/5 from the vitreous aspect.³³ As such, our evidence suggests that pre-retinal injection may only improve the transduction efficiency of AAV2-based vectors, wherein limiting diffusion is not sufficient in and of itself to facilitate transduction, and only vectors that bind HSPG are able to successfully traverse the ILM from the pre-retinal space.

The altered tropism observed after pre-retinal injection of rAAV was notable, with significantly greater numbers of cells in all retinal layers appearing to be transduced compared with animals given an equivalent or higher intravitreal dose volume of vector (Figure 3). Importantly, this increased transduction efficiency was associated with a significant increase in the number of transduced photoreceptor cells (Figure 5). One unexpected observation was that a subset of animals exhibited increased photoreceptor and inner retinal transduction in the absence of ganglion cell transduction (Figures 4B–4E), despite the use of the ubiquitous CBA promoter. This is in contrast to the other pre-retinally injected animals that exhibited pan-retinal transduction involving all retinal layers (Figure 4A). This observation remains unexplained but is particularly interesting in light of other studies that observed dramatically increased transduction of

ganglion cells and only modest increases in Müller glia, bipolar cell, and photoreceptor transduction following injection of rAAV directly underneath the ILM (sub-ILM injection), indicating that HSPG binding and traversal of the ILM may serve to increase retinal penetrance.^{33,34}

The distribution of vector across the retina differs markedly between delivery routes, with intravitreal injection of rAAV resulting primarily in transduction of cells in the area of the horizontal visual streak and around the vessels (Figures 2D and 2E). This finding is in accordance with numerous reports in other species and provides further evidence that composition of the ILM is critically important for rAAV transduction,^{35–39} where thinning of the ILM and increased Müller glia density in areas containing blood vessel results in increased penetrance and regional variation in transduction efficiency across the retina. By contrast, pre-retinal injection of rAAV resulted in near pan-retinal transduction that extends from the optic nerve head to the far periphery (Figures 2F and 4A), a finding that is consistent with observations made during surgery, where the posterior hyaloid membrane is seen to detach across the retina after vector administration (Figure S1; Video S1). Detachment of the posterior hyaloid membrane does not occur instantaneously at the moment of injection or result in a single defined bleb but occurs as a gradual “wave” spreading across the retina over a period of ~1 min after removal of the needle from the retinal surface. This raises the interesting question of whether the injection is directly hydro-dissecting the posterior hyaloid membrane from the ILM through force or whether rAAV is actually being drawn through the needle opening in the posterior hyaloid membrane from the extreme posterior vitreous and into the pre-retinal space, resulting in a gradual detachment and pan-retinal spread of the vector.

One concern regarding the pre-retinal delivery technique is that detachment of the posterior hyaloid membrane appears to be

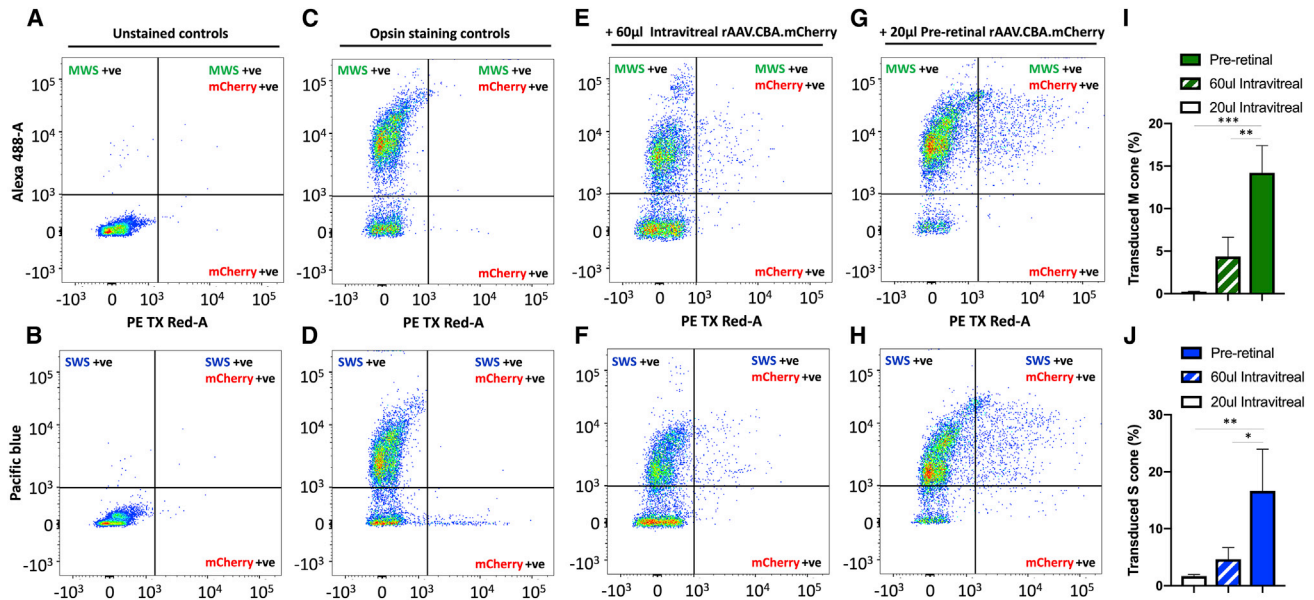


Figure 5. Quantification of cone photoreceptor transduction efficiency by flow cytometry

(A–H) Pseudocolor flow cytometry quadrant plots showing the transduced M-cone or S-cone of gating control (A–D), intravitreal administration (E and F), and pre-retinal administration (G and H) using the 488 nm (A, C, E, G) or violet laser (B, D, F, H), respectively. Transduction efficiency is expressed as the percentage of transduced M-cone (MWS+ve, mCherry+ve) and S-cone (SWS+ve, mCherry+ve) cells. (I and J) There are significant differences in transduction efficiency of both M-cone (I) and S-cone (J) between intravitreal administration and pre-retinal administration. Data are represented as mean \pm SD. * $p < 0.05$; ** $p < 0.01$; *** $p < 0.001$.

permanent in the 13-LGS model, and so we set out to evaluate whether this had any negative impact on either retinal structure or function. Importantly, despite the posterior hyaloid membrane remaining detached for a period of several weeks post-injection, no evidence of morphological changes (e.g., retinal thinning, atrophy) was observed with the use of a combination of OCT and cSLO imaging techniques. ERG conducted at several time points also revealed only a slight, but non-significant reduction in ERG amplitudes 4 weeks after vector administration. That detachment of the posterior hyaloid membrane is well tolerated and does not lead to vision loss was perhaps unsurprising, wherein posterior hyaloid separation/vitreous detachment is a naturally occurring phenomenon in humans that occurs as a result of aging, or as part of various retinal diseases, including uveitis, myopia, and diabetic retinopathy, without directly impacting visual acuity.^{28,40,41} Furthermore, a partial posterior hyaloidectomy, where the hyaloid membrane is intentionally detached during vitrectomy, is performed routinely as part of macular hole surgery in patients with diabetic or idiopathic retinopathy in order to limit traction and improve visual outcomes.^{42,43}

In summary, pre-retinal delivery of rAAV appears to be well tolerated in the 13-LGS and, even at a considerably lower dose volume, results in increased retinal transduction compared to the deep vitreous intravitreal delivery route. If developed further, the pre-retinal injection route could represent a novel method by which to administer gene therapy for the treatment of inherited retinal disease, particularly in younger patients with intact posterior hyaloid membranes and solid un-luified vitreous.^{44–46}

MATERIALS AND METHODS

Animal import, anesthesia, and experimental preparation

All animal experiments were conducted in accordance with the Association for Research in Vision and Ophthalmology (ARVO) Statement for the Use of Animals in Ophthalmic and Vision Research and with approval of the Medical College of Wisconsin (MCW) Institutional Animal Care and Use Committee (IACUC). Fourteen adult 13-LGSs (8 females, 6 males; Table 1) were obtained from the University of Wisconsin Oshkosh Squirrel Colony.¹⁹ All animals were kept on a natural photoperiod (12:12 to 14:10), with light on/off times updated every 2 weeks to reflect local seasonal shifts. All experiments were performed on euthermic (non-hibernating) animals under isoflurane anesthesia (5% induction, 1%–4% maintenance in 1 L/min oxygen flow) with mydriasis induced through the topical application of eye drops containing 1% tropicamide (Akorn, Lake Forest, IL, USA) and 2.5% phenylephrine HCL (Paragon BioTeck, Portland, OR, USA).

Recombinant adeno-associated virus production

rAAV vectors were manufactured as per our previously published protocol.⁴⁷ Briefly, HEK293T cells were seeded into HyperFlasks (Corning, New York, NY, USA) and triple transfected using a 2:1 PEI-to-DNA ratio with (1) a pTR plasmid containing a red fluorescent reporter protein (mCherry) expressed ubiquitously from a CBA promoter flanked by AAV2 inverted terminal repeats (ITRs); (2) a helper plasmid containing adenoviral elements (pHelper); and (3) a plasmid encoding AAV2 Rep and Cap genes for a mutant capsid, termed rAAV2/2[*MAX*], that contains five previously elucidated point

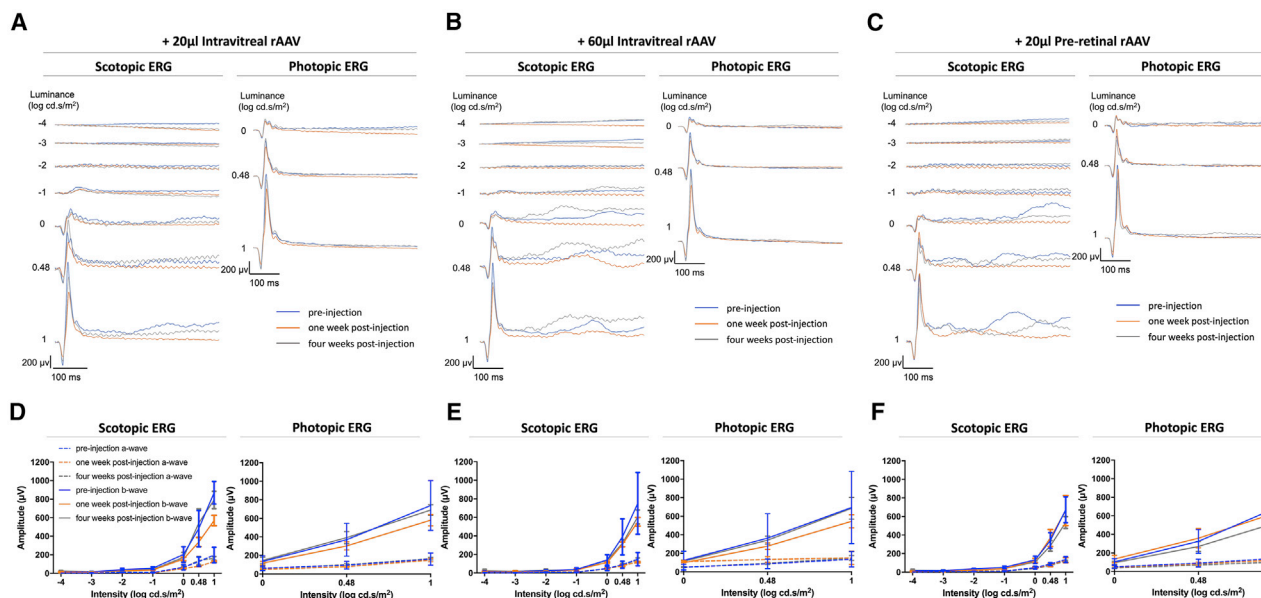


Figure 6. Full-field ERG on 13-LGS eyes that received intravitreal or pre-retinal vector injection

(A) Representative ERG traces pre (blue)-, 1 week post (orange)-, and 4 weeks post (gray)-intravitreal injection of 20 µL rAAV. (B) Representative ERG traces pre (blue)-, 1 week post (orange)-, and 4 weeks post (gray)-intravitreal injection of 60 µL rAAV. (C) Representative ERG traces pre (blue)-, 1 week post (orange)-, and 4 weeks post (gray)-pre-retinal injection of 20 µL rAAV. The ERG protocol includes scotopic single-flash ERG with increased stimulus luminance (−4 to 1 log cd·s/m²) and photopic single-flash ERG with increased stimulus luminance (0, 0.48, 1 log cd·s/m²). (D–F) There is no significant change among different time points of the a- and b-wave amplitudes for any injection routes and injected dose volumes. Data are shown as mean ± SD. Repeated-measures two-way ANOVA with Tukey post hoc assay was used for statistical analysis.

mutations (QuadYF-TV) and the 7m8 peptide insertion.^{10,13,14,48} Three days post-transfection, cells were harvested, lysed, and purified via iodixanol ultra-centrifugation followed by buffer exchange using a 100 kDa centrifugation column (Amicon, Darmstadt, Germany) into HBSS containing 0.014% Tween 20.⁴⁹ The rAAV titer was determined with a PicoGreen assay as described previously.⁵⁰

Intraocular injections

Twenty 13-LGSs (n = 32 eyes; Table 1) received injections of rAAV2/2 [MAX].CBA.mCherry, rAAV2/5.CBA.mCherry, or HBSS via either an intravitreal or pre-retinal injection route under visualization of an ophthalmic microscope (Leica, Wetzlar, Germany). Briefly, intravitreal injections were performed by advancing a 10 mm sharp-ended (point

style 2) 33G needle (Hamilton, Franklin, MA, USA) attached to a 100 µL Hamilton syringe trans-sclerally ~1 mm posterior to the limbus. The needle tip was carefully advanced into the mid-deep vitreous over the area of the visual streak and immediately inferior to the horizontal optic nerve head, where the vector was injected manually over a period of up to 1 min (depending on volume). After injection, intraocular pressure (IOP) was allowed to normalize in order to limit reflux before the needle was withdrawn from the globe. Pre-retinal injections were performed by first opening a scleral port ~1 mm posterior to the limbus at the medial canthus with a 27G trocar blade (without cannula). A 12 mm blunt-ended (point style 3) 33G needle (Hamilton, Franklin, MA, USA) with manually bent tip attached to a 100 µL Hamilton syringe was advanced through the scleral port until the bent needle tip made contact with the retina and entered the pre-retinal space. A 20 µL volume of either vector or HBSS was manually injected over a period of ~10 s prior to the needle being withdrawn to the deep vitreous to allow for IOP equalization, before being removed from the globe. A detailed description of the pre-retinal injection procedure is provided in Figure S1 and in the accompanying Video S1.

Ocular imaging

After anesthesia and mydriasis, corneal hydration was maintained throughout all imaging procedures via the periodic application of topical eye drops (Allergan, Dublin, Ireland) to prevent desiccation and maintain corneal clarity. A custom multiline cSLO based on the Spectralis HRA (Heidelberg Engineering, Heidelberg, Germany) was used to obtain NIR (810–820 nm excitation) and red fluorescent

Table 2. Cone transduction efficiency of rAAV2/2[MX].CBA.mCherry using traditional intravitreal injection versus pre-retinal injection, evaluated using flow cytometry of papain-dissociated 13-LGS retinae

Route	Intravitreal		Pre-retinal
Volume	20 µL (2 × 10 ¹¹ vg)	60 µL (6 × 10 ¹¹ vg)	20 µL (2 × 10 ¹¹ vg)
M-cone transduction (significance versus pre-retinal)	0.21% (p = 0.0003)	4.99% (p = 0.0041)	14.2%
S-cone transduction (significance versus pre-retinal)	1.68% (p = 0.0125)	5.44% (p = 0.0464)	16.63%

Even at a higher dose volume, pre-retinal delivery significantly outperformed intravitreal delivery.

(561 ± 2 nm excitation) images of the squirrel fundus. OCT imaging of the retina was performed with the Bioptigen Envisu R2200 Spectral Domain OCT system (Leica Microsystems, Wetzlar, Germany) equipped with a Superlum Broadlighter T-870 light source (λ_0 : 878.4 nm, $\Delta\lambda$: 186.3 nm; Superlum, Cork, Ireland). Volume scans (650 A-scans × 650 A-scans/B-scan) were acquired for each animal, and images were processed by averaging 4 adjacent frames/B-scans.

Cryosection and immunostaining

13-LGSs were euthanized by decapitation without recovering from anesthesia, as described previously, and the globes enucleated.⁵¹ After harvesting of the globes, the cornea and lens were removed, and the eyecups were fixed in 4% paraformaldehyde prior to cryopreservation in 30% sucrose at 4°C overnight. Eyecups were subsequently embedded in optical cutting temperature medium (OCT), and 12 μm sections were made with a cryostat microtome system (Leica, Wetzlar, Germany). Sections were dried overnight before being transferred to storage at -20°C prior to processing. Sections were permeabilized with 0.2% Triton X for 20 min prior to blocking in 6% normal donkey serum and 1% BSA in 0.1% Triton X in PBS for 1 h. mCherry signal was amplified using a 1:200 dilution of anti-dsRed antibody (Santa Cruz, Dallas, TX, USA), and sections were incubated at 4°C overnight. After incubation, sections were washed three times with 0.1% PBS-Tween (PBST) and incubated in donkey anti-mouse Alexa Fluor 555 secondary antibody (1:400, Life Technologies, Carlsbad, CA, USA) at room temperature for 1 h. Samples were washed with PBS three times for 30 min and counterstained with Hoechst 33342 (1:1,000, Life Technologies, Carlsbad, CA, USA). Slides were imaged on a confocal microscope (Nikon Eclipse 80i; Nikon, Minato, Tokyo, Japan) with either a 20× or 40× objective with 405 nm and 561 nm lasers (Coherent, Santa Clara, CA, USA). Z stack and merged channel images were processed by Fiji software.⁵²

Flow cytometry

13-LGSs were euthanized by decapitation under terminal isoflurane anesthesia prior to enucleation of the globes and dissection of the neural retina into small fragments with vannas scissors (Fine Science Tools, Heidelberg, Germany). Enzymatic dissociation of 13-LGS retina fragments was performed with papain (Worthington, Lakewood, NJ, USA), as described previously.¹⁴ After dissociation, cells were incubated on ice for 1 h under gentle rocking with chicken anti-MWS opsin (JH 6105) and rabbit anti-SWS opsin (JH 455) antisera (a kind gift from Dr. Jeremy Nathans, Johns Hopkins) at a concentration of 1:200 in PBST containing 3% BSA. After washing (FACS buffer), cells were incubated with goat anti-chicken Alexa Fluor 488 (1:200 in 3% BSA, Molecular Probes, Eugene, OR, USA) and goat anti-rabbit Alexa Fluor 405 (1:200 in 3% BSA, Invitrogen, Carlsbad, CA, USA) secondary antibodies at 4°C for 1 h. The expression of mCherry, MWS opsin, and SWS opsin was then quantified with a BD LSRII flow cytometer (Franklin Lakes, NJ, USA). Dissociated cells harvested from a sham-injected 13-LGS were used to generate the following gating controls: no antibody (unstained) and single primary antibody (MWS and SWS opsin separately). Part of the dissociated cells harvested from vector-injected 13-LGS without antibody stain-

ing were used as a Texas red gating control. Ten thousand events were recorded for each sample in FACSDiva software (BD Biosciences, San Jose, CA, USA). Further analysis of the samples of graphical display of the results was completed with cytometry data analysis software (FlowJo, Ashland, OR, USA).

Full-field ERG

Animals were dark-adapted 30 min prior to ERG recording and handled under red dim light throughout the procedure. The experiment was performed on an Espion E2 system (Diagnosys LLC, Cambridge, UK) as previously described.¹⁸ Briefly, ground electrodes were inserted at the scalp and haunch, and reference electrodes were positioned on the corneal surface of both eyes. The scotopic ERG includes 5-log series single-flash stimuli with gradually increased luminance (-4 to 1 log cd·s/m²). After 10 min light adaptation in a 25 cd/m² white background, photopic ERGs were performed with gradually increased single-flash stimuli (0-, 0.48- and 1-log cd·s/m²). For ERG data analysis, a- and b-waveforms were manually identified by Diagnosys Espion E3. The amplitude values were exported into GraphPad Prism 8 for statistical analysis.

Statistical analysis

For the flow cytometry analysis, one-way ANOVA with Tukey post hoc assay was used for comparing the numbers of transduced photoreceptors between injection routes and volumes, with a confidence level of 95% ($\alpha = 0.05$). For ERG analysis, two-way ANOVA with Tukey post hoc assay with a 95% confidence interval ($\alpha = 0.05$) was used for comparing a- and b-wave amplitudes pre-, 1 week post-, and 4 weeks post-injection.

SUPPLEMENTAL INFORMATION

Supplemental information can be found online at <https://doi.org/10.1016/j.omtm.2021.06.005>.

ACKNOWLEDGMENTS

The authors thank Christine Skumatz, Lisa King, Joseph Thulin, and the Biomedical Resource Center staff for their help with animal care. This work was supported by grants from the National Eye Institute (U24EY029891 and R01EY027767) and the Foundation for Fighting Blindness (PPA-0641-0718-UCSF and TA-NMT-0618-0739). This investigation was conducted in part in a facility constructed with support from a Research Facilities Improvement Program (C06RR016511) from the National Center for Research Resources of the National Institutes of Health. The content is solely the responsibility of the authors and does not necessarily represent the official views of the National Institutes of Health.

AUTHOR CONTRIBUTIONS

H.Z. and D.M.L. designed and conducted the experiments and wrote the paper. B.S.S. helped conduct the experiments and reviewed the manuscript. D.K.M. and J.C. provided access to the 13-LGS model and reviewed the manuscript.

DECLARATION OF INTERESTS

The authors declare no competing interests.

REFERENCES

- Jacobson, S.G., Cideciyan, A.V., Ratnakaram, R., Heon, E., Schwartz, S.B., Roman, A.J., Peden, M.C., Aleman, T.S., Boye, S.L., Sumaroka, A., et al. (2012). Gene therapy for leber congenital amaurosis caused by RPE65 mutations: safety and efficacy in 15 children and adults followed up to 3 years. *Arch. Ophthalmol.* *130*, 9–24.
- Nuzbrokh, Y., Kassotis, A.S., Ragi, S.D., Jauregui, R., and Tsang, S.H. (2020). Treatment-Emergent Adverse Events in Gene Therapy Trials for Inherited Retinal Diseases: A Narrative Review. *Ophthalmol. Ther.* *9*, 709–724.
- Heier, J.S., Brown, D.M., Chong, V., Korobelnik, J.F., Kaiser, P.K., Nguyen, Q.D., Kirchhof, B., Ho, A., Ogura, Y., Yancopoulos, G.D., et al.; VIEW 1 and VIEW 2 Study Groups (2012). Intravitreal aflibercept (VEGF trap-eye) in wet age-related macular degeneration. *Ophthalmology* *119*, 2537–2548.
- Cheung, N., Wong, I.Y., and Wong, T.Y. (2014). Ocular anti-VEGF therapy for diabetic retinopathy: overview of clinical efficacy and evolving applications. *Diabetes Care* *37*, 900–905.
- Dalkara, D., Kolstad, K.D., Caporale, N., Visel, M., Klimczak, R.R., Schaffer, D.V., and Flannery, J.G. (2009). Inner limiting membrane barriers to AAV-mediated retinal transduction from the vitreous. *Mol. Ther.* *17*, 2096–2102.
- Kotterman, M.A., Yin, L., Strazzeri, J.M., Flannery, J.G., Merigan, W.H., and Schaffer, D.V. (2015). Antibody neutralization poses a barrier to intravitreal adeno-associated viral vector gene delivery to non-human primates. *Gene Ther.* *22*, 116–126.
- Dias, M.S., Araujo, V.G., Vasconcelos, T., Li, Q., Hauswirth, W.W., Linden, R., and Peters-Silva, H. (2019). Retina transduction by rAAV2 after intravitreal injection: comparison between mouse and rat. *Gene Ther.* *26*, 479–490.
- Peters-Silva, H., Dinculescu, A., Li, Q., Deng, W.T., Pang, J.J., Min, S.H., Chiodo, V., Neeley, A.W., Govindasamy, L., Bennett, A., et al. (2011). Novel properties of tyrosine-mutant AAV2 vectors in the mouse retina. *Mol. Ther.* *19*, 293–301.
- Peters-Silva, H., Dinculescu, A., Li, Q., Min, S.H., Chiodo, V., Pang, J.J., Zhong, L., Zolotukhin, S., Srivastava, A., Lewin, A.S., and Hauswirth, W.W. (2009). High-efficiency transduction of the mouse retina by tyrosine-mutant AAV serotype vectors. *Mol. Ther.* *17*, 463–471.
- Kay, C.N., Ryals, R.C., Aslanidi, G.V., Min, S.H., Ruan, Q., Sun, J., Dyka, F.M., Kasuga, D., Ayala, A.E., Van Vliet, K., et al. (2013). Targeting photoreceptors via intravitreal delivery using novel, capsid-mutated AAV vectors. *PLoS ONE* *8*, e62097.
- Grifman, M., Trepel, M., Speece, P., Gilbert, L.B., Arap, W., Pasqualini, R., and Weitzman, M.D. (2001). Incorporation of tumor-targeting peptides into recombinant adeno-associated virus capsids. *Mol. Ther.* *3*, 964–975.
- Girod, A., Ried, M., Wobus, C., Lahm, H., Leike, K., Kleinschmidt, J., Deléage, G., and Hallek, M. (1999). Genetic capsid modifications allow efficient re-targeting of adeno-associated virus type 2. *Nat. Med.* *5*, 1052–1056.
- Dalkara, D., Byrne, L.C., Klimczak, R.R., Visel, M., Yin, L., Merigan, W.H., Flannery, J.G., and Schaffer, D.V. (2013). In vivo-directed evolution of a new adeno-associated virus for therapeutic outer retinal gene delivery from the vitreous. *Sci. Transl. Med.* *5*, 189ra76.
- Reid, C.A., Ertel, K.J., and Lipinski, D.M. (2017). Improvement of photoreceptor targeting via intravitreal delivery in mouse and human retina using combinatory rAAV2 capsid mutant vectors. *Invest. Ophthalmol. Vis. Sci.* *58*, 6429–6439.
- Zeng, Y., Boyd, R., Bartoe, J., Wiley, H.E., Marangoni, D., Wei, L.L., and Sieving, P.A. (2020). “Para-retinal” Vector Administration into the Deep Vitreous Enhances Retinal Transgene Expression. *Mol. Ther. Methods Clin. Dev.* *18*, 422–427.
- Verra, D.M., Sajdak, B.S., Merriman, D.K., and Hicks, D. (2020). Diurnal rodents as pertinent animal models of human retinal physiology and pathology. *Prog. Retin. Eye Res.* *74*, 100776.
- Sajdak, B., Sulai, Y.N., Langlo, C.S., Luna, G., Fisher, S.K., Merriman, D.K., and Dubra, A. (2016). Noninvasive imaging of the thirteen-lined ground squirrel photoreceptor mosaic. *Vis. Neurosci.* *33*, e003.
- Zhang, H., Sajdak, B.S., Merriman, D.K., McCall, M.A., Carroll, J., and Lipinski, D.M. (2020). Electroretinogram of the cone-dominant thirteen-lined ground squirrel during Euthermia and Hibernation in comparison with the rod-dominant Brown Norway rat. *Invest. Ophthalmol. Vis. Sci.* *61*, 6.
- Merriman, D.K., Lahvis, G., Jooss, M., Gesicki, J.A., and Schill, K. (2012). Current practices in a captive breeding colony of 13-lined ground squirrels (*Ictidomys tridecemlineatus*). *Lab Anim. (NY)* *41*, 315–325.
- Zygmunt, D.A., Crowe, K.E., Flanigan, K.M., and Martin, P.T. (2017). Comparison of Serum rAAV Serotype-Specific Antibodies in Patients with Duchenne Muscular Dystrophy, Becker Muscular Dystrophy, Inclusion Body Myositis, or GNE Myopathy. *Hum. Gene Ther.* *28*, 737–746.
- Ronzitti, G., Gross, D.A., and Mingozzi, F. (2020). Human Immune Responses to Adeno-Associated Virus (AAV) Vectors. *Front. Immunol.* *11*, 670.
- Kokona, D., Häner, N.U., Ebnetter, A., and Zinkernagel, M.S. (2017). Imaging of macrophage dynamics with optical coherence tomography in anterior ischemic optic neuropathy. *Exp. Eye Res.* *154*, 159–167.
- Kato, M., Koike, Y., Suzuki, S., and Kimata, K. (1988). Basement membrane proteoglycan in various tissues: characterization using monoclonal antibodies to the Engelbreth-Holm-Swarm mouse tumor low density heparan sulfate proteoglycan. *J. Cell Biol.* *106*, 2203–2210.
- Boye, S.L., Bennett, A., Scalabrino, M.L., McCullough, K.T., Van Vliet, K., Choudhury, S., Ruan, Q., Peterson, J., Agbandje-McKenna, M., and Boye, S.E. (2016). Impact of Heparan Sulfate Binding on Transduction of Retina by Recombinant Adeno-Associated Virus Vectors. *J. Virol.* *90*, 4215–4231.
- Cehajic-Kapetanovic, J., Milosavljevic, N., Bedford, R.A., Lucas, R.J., and Bishop, P.N. (2017). Efficacy and Safety of Glycosidic Enzymes for Improved Gene Delivery to the Retina following Intravitreal Injection in Mice. *Mol. Ther. Methods Clin. Dev.* *9*, 192–202.
- Cehajic-Kapetanovic, J., Le Goff, M.M., Allen, A., Lucas, R.J., and Bishop, P.N. (2011). Glycosidic enzymes enhance retinal transduction following intravitreal delivery of AAV2. *Mol. Vis.* *17*, 1771–1783.
- Heegaard, S., Jensen, O.A., and Prause, J.U. (1986). Structure and composition of the inner limiting membrane of the retina. SEM on frozen resin-cracked and enzyme-digested retinas of *Macaca mulatta*. *Graefes Arch. Clin. Exp. Ophthalmol.* *224*, 355–360.
- Fincham, G.S., James, S., Spickett, C., Hollingshead, M., Thrasivoulou, C., Poulson, A.V., McNinch, A., Richards, A., Snead, D., Limb, G.A., and Snead, M.P. (2018). Posterior Vitreous Detachment and the Posterior Hyaloid Membrane. *Ophthalmology* *125*, 227–236.
- Tao, C., and Zhang, X. (2016). Retinal Proteoglycans Act as Cellular Receptors for Basement Membrane Assembly to Control Astrocyte Migration and Angiogenesis. *Cell Rep.* *17*, 1832–1844.
- Di Pasquale, G., Davidson, B.L., Stein, C.S., Martins, I., Scudiero, D., Monks, A., and Chiorini, J.A. (2003). Identification of PDGFR as a receptor for AAV-5 transduction. *Nat. Med.* *9*, 1306–1312.
- Beltran, W.A., Boye, S.L., Boye, S.E., Chiodo, V.A., Lewin, A.S., Hauswirth, W.W., and Aguirre, G.D. (2010). rAAV2/5 gene-targeting to rods: dose-dependent efficiency and complications associated with different promoters. *Gene Ther.* *17*, 1162–1174.
- Kaludov, N., Brown, K.E., Walters, R.W., Zabner, J., and Chiorini, J.A. (2001). Adeno-associated virus serotype 4 (AAV4) and AAV5 both require sialic acid binding for hemagglutination and efficient transduction but differ in sialic acid linkage specificity. *J. Virol.* *75*, 6884–6893.
- Boye, S.E., Alexander, J.J., Witherspoon, C.D., Boye, S.L., Peterson, J.J., Clark, M.E., Sandefer, K.J., Girkin, C.A., Hauswirth, W.W., and Gamlin, P.D. (2016). Highly efficient delivery of adeno-associated viral vectors to the primate retina. *Hum. Gene Ther.* *27*, 580–597.
- Takahashi, K., Igarashi, T., Miyake, K., Kobayashi, M., Yaguchi, C., Iijima, O., Yamazaki, Y., Katakai, Y., Miyake, N., Kameya, S., et al. (2017). Improved Intravitreal AAV-Mediated Inner Retinal Gene Transduction after Surgical Internal Limiting Membrane Peeling in Cynomolgus Monkeys. *Mol. Ther.* *25*, 296–302.
- Vacca, O., Darche, M., Schaffer, D.V., Flannery, J.G., Sahel, J.A., Rendon, A., and Dalkara, D. (2014). AAV-mediated gene delivery in Dp71-null mouse model with compromised barriers. *Glia* *62*, 468–476.

36. Mowat, F.M., Gornik, K.R., Dinculescu, A., Boye, S.L., Hauswirth, W.W., Petersen-Jones, S.M., and Bartoe, J.T. (2014). Tyrosine capsid-mutant AAV vectors for gene delivery to the canine retina from a subretinal or intravitreal approach. *Gene Ther.* *21*, 96–105.
37. Wolter, J.R. (1964). Pores in the internal limiting membrane of the human retina. *Acta Ophthalmol. (Copenh.)* *42*, 971–974.
38. Distler, C., and Dreher, Z. (1996). Glia cells of the monkey retina—II. Müller cells. *Vision Res.* *36*, 2381–2394.
39. Yin, L., Greenberg, K., Hunter, J.J., Dalkara, D., Kolstad, K.D., Masella, B.D., Wolfe, R., Visel, M., Stone, D., Libby, R.T., et al. (2011). Intravitreal injection of AAV2 transduces macaque inner retina. *Invest. Ophthalmol. Vis. Sci.* *52*, 2775–2783.
40. Ștefănescu-Dima, A.Ș., Corici, C.A., Mănescu, M.R., Sas, T.N., Iancău, M., and Mocanu, C.L. (2016). Posterior vitreous detachment and macular anatomical changes - a tomographic-electroretinographic study. *Rom. J. Morphol. Embryol.* *57* (2, Suppl), 751–758.
41. Kakehashi, A., Kado, M., Akiba, J., and Hirokawa, H. (1997). Variations of posterior vitreous detachment. *Br. J. Ophthalmol.* *81*, 527–532.
42. Özkan, B., Karabaş, V.L., Yılmaz Tuğan, B., and Altıntaş, Ö. (2019). Limited vitrectomy in patients with idiopathic macular hole. *Balkan Med. J.* *36*, 320–323.
43. Kim, J.H., Kang, S.W., Kim, Y.T., Kim, S.J., and Chung, S.E. (2013). Partial posterior hyaloidectomy for macular disorders. *Eye (Lond.)* *27*, 946–951.
44. Harocopos, G.J., Shui, Y.B., McKinnon, M., Holekamp, N.M., Gordon, M.O., and Beebe, D.C. (2004). Importance of vitreous liquefaction in age-related cataract. *Invest. Ophthalmol. Vis. Sci.* *45*, 77–85.
45. Sebag, J. (1987). Age-related changes in human vitreous structure. *Graefes Arch. Clin. Exp. Ophthalmol.* *225*, 89–93.
46. Sebag, J. (1991). Age-related differences in the human vitreoretinal interface. *Arch. Ophthalmol.* *109*, 966–971.
47. Reid, C.A., and Lipinski, D.M. (2018). Small and micro-scale recombinant adeno-associated virus production and purification for ocular gene therapy applications. *Methods Mol. Biol.* *1715*, 19–31.
48. Cashman, S.M., McCullough, L., and Kumar-Singh, R. (2007). Improved retinal transduction in vivo and photoreceptor-specific transgene expression using adeno-virus vectors with modified penton base. *Mol. Ther.* *15*, 1640–1646.
49. Zolotukhin, S., Byrne, B.J., Mason, E., Zolotukhin, I., Potter, M., Chesnut, K., Summerford, C., Samulski, R.J., and Muzyczka, N. (1999). Recombinant adeno-associated virus purification using novel methods improves infectious titer and yield. *Gene Ther.* *6*, 973–985.
50. Piedra, J., Ontiveros, M., Miravet, S., Penalva, C., Monfar, M., and Chillón, M. (2015). Development of a rapid, robust, and universal picogreen-based method to titer adeno-associated vectors. *Hum. Gene Ther. Methods* *26*, 35–42.
51. Sajdak, B.S., Bell, B.A., Lewis, T.R., Luna, G., Cornwell, G.S., Fisher, S.K., Merriman, D.K., and Carroll, J. (2018). Assessment of Outer Retinal Remodeling in the Hibernating 13-Lined Ground Squirrel. *Invest. Ophthalmol. Vis. Sci.* *59*, 2538–2547.
52. Schroeder, A.B., Dobson, E.T.A., Rueden, C.T., Tomancak, P., Jug, F., and Eliceiri, K.W. (2021). The ImageJ ecosystem: Open-source software for image visualization, processing, and analysis. *Protein Sci.* *30*, 234–249.